Physics Letters B 750 (2015) 356–359

Contents lists available at ScienceDirect

Physics Letters B

www.elsevier.com/locate/physletb

Systematic trends in beta-delayed particle emitting nuclei: The case of $\beta p\alpha$ emission from ^{21}Mg

M.V. Lund [a,*], M.J.G. Borge [b,c], J.A. Briz [c], J. Cederkäll [d], H.O.U. Fynbo [a], J.H. Jensen [a], B. Jonson [e], K.L. Laursen [a], T. Nilsson [e], A. Perea [c], V. Pesudo [c], K. Riisager [a], O. Tengblad [c]

[a] Department of Physics and Astronomy, Aarhus University, DK-8000, Aarhus C, Denmark
[b] ISOLDE, PH Department, CERN, CH-1211 Geneve 23, Switzerland
[c] Instituto de Estructura de la Materia, CSIC, E-28006 Madrid, Spain
[d] Department of Nuclear Physics, Lund University, SE-221 00 Lund, Sweden
[e] Fundamental Fysik, Chalmers Tekniska Högskola, SE-41296 Göteborg, Sweden

ARTICLE INFO

Article history:
Received 12 June 2015
Received in revised form 11 September 2015
Accepted 16 September 2015
Available online 25 September 2015
Editor: D.F. Geesaman

Keywords:
Beta decay
Multi-particle emission
^{21}Mg

ABSTRACT

We have observed β^+-delayed α and pα emission from the proton-rich nucleus ^{21}Mg produced at the ISOLDE facility at CERN. The assignments were cross-checked with a time distribution analysis. This is the third identified case of $\beta p\alpha$ emission. We discuss the systematic of beta-delayed particle emission decays, show that our observed decays fit naturally into the existing pattern, and argue that the patterns are to a large extent caused by odd–even effects.

1. Introduction

Beta-delayed particle emission is an important decay mode for exotic nuclei and allows many aspects of nuclear structure to be probed, see the two recent reviews [1,2] for a comprehensive overview. We report here the first observation of $\beta\alpha$ emission as well as the rare $\beta p\alpha$ emission from the nucleus ^{21}Mg. Based on these observations we have identified systematic patterns in the occurrence of beta-delayed particle decays in proton-rich nuclei. We shall present and discuss these as well.

A detailed description of beta-delayed particle emission must include consideration of local nuclear structure effects, but its occurrence is in general dominated by the available energy, i.e. the difference between the Q_β-value and the particle separation energy. As is well known, for an isobaric chain with mass number A the Q_β values will increase and the proton and neutron separation energies decrease as one moves from the beta stability line towards the driplines (modulated for even A by the pairing term). The α particle separation energy tends for light nuclei to be minimal for $N = Z$ nuclei, but the minimum moves towards more proton rich nuclei and reaches the proton dripline at $A \sim 50$. This causes a clear pattern for beta-delayed multi-particle emission, with β2p and β3p taking place close to the proton dripline, β2n, β3n etc. starting from about halfway to the neutron dripline, while $\beta 2\alpha$ is seen from $A = 8, 9, 12$ nuclei close to stability. (To the extent that these decays are sequential one can of course regard them as $\beta\alpha$ decays to the unstable $A = 5, 8$ nuclei.) Similar patterns appear in beta-delayed single-particle emission although exceptions occur for the very light nuclei such as the large P_n values for $N = 10$ nuclei and the $\beta\alpha$ emission from neutron-rich N-isotopes.

We focus first on the multi-particle $\beta p\alpha$ decay and return in the discussion to the general patterns of beta-delayed particle emission.

2. Experimental results

The ^{21}Mg activity was produced at the ISOLDE facility at CERN by a 1.4 GeV proton beam impinging upon a SiC target. The produced atoms were extracted, laser ionized, accelerated to 60 keV, led through a mass separator into the experimental set-up, and implanted in the window of a gas-Si telescope opposed by a Si(DSSSD)-Si telescope. A full account of the experimental

* Corresponding author.
E-mail address: mvl07@phys.au.dk (M.V. Lund).

http://dx.doi.org/10.1016/j.physletb.2015.09.044

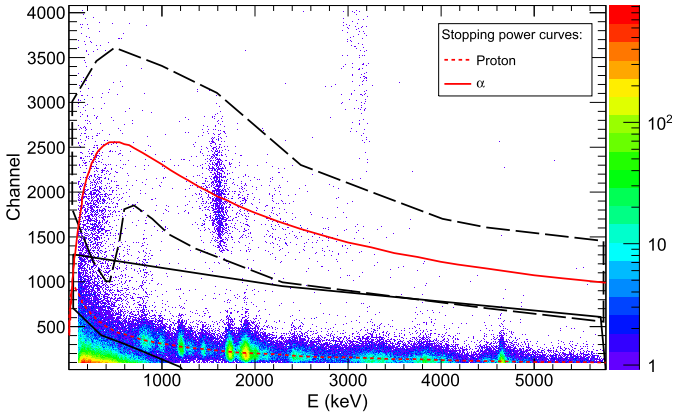

Fig. 1. (Color online.) ΔE–E plot from the Gas-Si telescope with the gas channel on the vertical axis and the deposited energy in the silicon detector on the horizontal axis. The scaled stopping powers for α's and protons are shown on top of the data in solid and dashed red, respectively. The graphical cut used for the α-particles is shown with the dashed black closed line and the cut for the protons is shown by the solid black closed line. The events with 3.18 MeV in the silicon detector and high energy deposition in the gas are due to a contamination of ^{148}Gd.

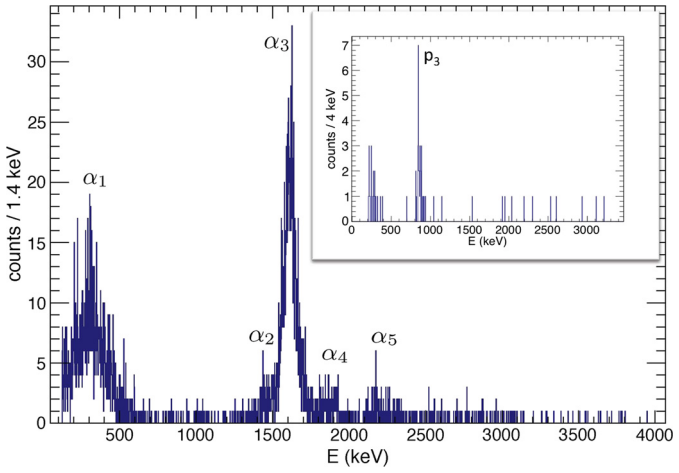

Fig. 2. (Color online.) Singles α spectrum extracted from the Gas-Si telescope. The inset in the top right corner shows the DSSSD proton spectrum in coincidence with the low energy α_1 line.

procedure is given in [3]. The collected source also contained a substantial amount of ^{21}Na.

The data from the Gas-Si charged particle telescope are presented as a ΔE–E spectrum in Fig. 1. Rescaled stopping powers [4] for α particles and protons (evaluated for silicon, but representing the total energy loss in the collection foil, the gas detector and the Si dead layer) are drawn in the figure and match the data well, indicating the presence of $\beta\alpha$ decays on top of the previously established [5,6] βp. The β-particle component in the lower left corner of Fig. 1 overlaps with protons below 1150 keV and α-particles below 700 keV making particle identification difficult at low energy. The α-particles are stopped in the DSSSD and cannot be separated there from the more intense proton branches.

The α-particle spectrum extracted from the gas-telescope by applying the gate drawn as a dashed black closed line in Fig. 1 is shown in Fig. 2. Apart from a remaining background component at low energy five α branches can be identified in the spectrum. The α_2, α_3, α_4 and α_5 lines naturally fit into the ^{21}Mg scheme put forward in [3] as β-delayed single α branches (see decay scheme in Fig. 3). The α_1 line, with measured laboratory energy 714(12) keV, does not fit with a transition between known levels in ^{21}Na and ^{17}F. However, it does agree with a known α-particle

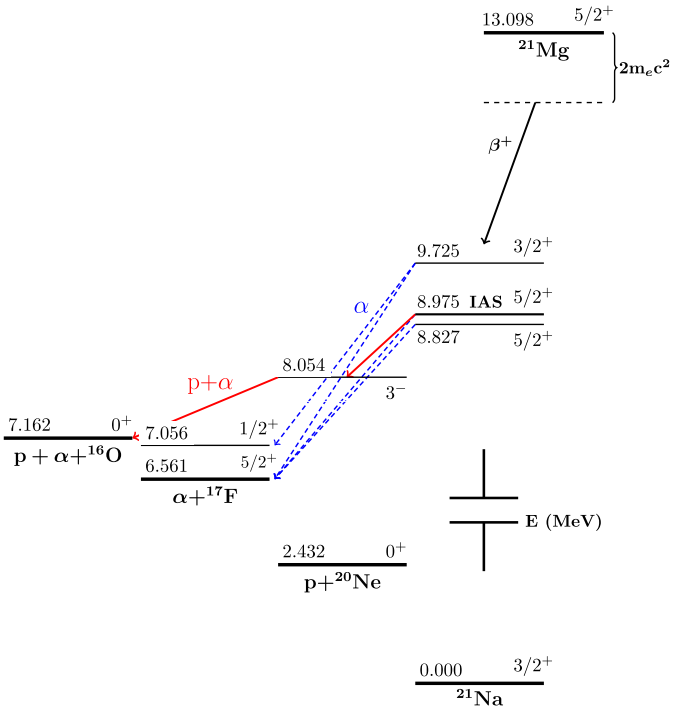

Fig. 3. (Color online.) Decay scheme focused on the ^{21}Mg($\beta\alpha$) and ^{21}Mg($\beta p\alpha$) decay modes.

transition from ^{20}Ne to ^{16}O observed in the decay of ^{20}Na [7] with a laboratory energy of 714(4) keV.

A conclusive particle identification for α_1 was not possible from the ΔE–E plot, but strong support for the above assignment comes from the observation of a coincident line in the DSSSD detector, assigned to be the preceding proton. This proton branch p_3 (the numbering is chosen to be consistent with the full data set discussed in [3]) is displayed as the inset in Fig. 2. From the measured energy we deduce $E_{cm}(p_3) = 919(18)$ keV which leads to the interpretation of α_1 and p_3 as being due to $\beta p\alpha$ decay of ^{21}Mg through the $5/2^+$ isobaric analogue state (IAS) at 8.975 MeV in ^{21}Na via proton emission to the 5.621 MeV 3^- level in ^{20}Ne and finally α emission to the ground state of ^{16}O. The total branching ratio of this decay branch is found to be $1.6(3) \cdot 10^{-4}$. This proton branch from the IAS has not been observed earlier and α-emission from excited states of ^{21}Na have only been reported in one earlier experiment [8].

2.1. Time distribution analysis

As mentioned above our data are contaminated by ^{21}Na, other small contaminants could in principle also be present. The observed $\beta\alpha$ and $\beta p\alpha$ branches are quite weak, so a cross-check of the assignment is valuable. This is done by considering the time distribution of the events.

Several factors influence the time distribution of the recorded ^{21}Mg events, see [3] for an exhaustive discussion. We shall use as reference the experimental time distribution recorded for events within the proton gate in Fig. 1 and with energy above 1150 keV. The energy gate ensures that the reference distribution only contains protons from the decay of ^{21}Mg. The halflives of ^{21}Mg and ^{21}Na, 122(2) ms and 22.49(4) s [9], differ greatly as do the corresponding time distributions. Other contaminants are also expected to differ from ^{21}Mg.

Some of the $\beta\alpha$ branches have quite low statistics and we therefore compare their time distribution directly to the reference

Table 1
EDF goodness-of-fit tests of the time distribution of the individual observed lines. The first column denotes the test, the second column gives the 95% confidence level (obtained through Monte Carlo simulations) for having the ^{21}Mg time distribution.

	95% c.l.	p_3	α_1	α_2, α_3	α_4	α_5
D	1.31	1.22	1.64	0.64	1.08	0.81
W^2	0.46	0.33	0.41	0.05	0.33	0.12
A^2	2.49	1.46	3.61	0.64	1.73	0.80

distribution. This can be done very efficiently with the empirical distribution function (EDF) statistics [10] that give powerful goodness-of-fit tests. The basic principle is to compare the shape of the data sample to the reference shape by measuring the distance between the two cumulated distributions. For experimental and reference distributions with values EDF_i and F_i in bin i, the three most frequently used EDF statistics are [11] Kolmogorov–Smirnov

$$D = \sqrt{N} \max_i |EDF_i - F_i|,$$

Cramer–Von Mises

$$W^2 = N \sum_i (EDF_i - F_i)^2 p_i$$

and Anderson–Darling

$$A^2 = N \sum_i \frac{(EDF_i - F_i)^2 p_i}{F_i(1 - F_i)},$$

where N is the total number of counts and p_i is the probability to be in bin i in the reference distribution. The second column of Table 1 gives the 95% confidence levels for the three EDF statistics obtained through Monte Carlo simulation, values below these levels indicate the time distribution for the different lines are consistent with the one of ^{21}Mg. More details on the confidence levels are given in [3].

The EDF test results in Table 1 show that all lines, except for α_1, agree with the reference distribution. The agreement is particularly good for the strongest line, α_3. As mentioned above there is a contamination of β-particles in α_1 that come from both ^{21}Na and ^{21}Mg. We would therefore expect the time distribution for α_1 to be mainly that of ^{21}Mg with a small component of ^{21}Na. The EDF tests are sufficiently sensitive to see the effect of the small ^{21}Na contribution. We expect, and do observe, that the upper part of the α_1 distribution has smaller contamination level. The fact that the coincident p_3 distribution is consistent with being from ^{21}Mg implies that we can safely assign the $\beta p\alpha$ transition, as well as all $\beta\alpha$ transitions, to the decay of ^{21}Mg.

3. Discussion

3.1. Other $\beta p\alpha$ cases

The $\beta p\alpha$ decay mode is very rare as described in [1] with only two previously established cases: ^{9}C and ^{17}Ne. For two further candidates, ^{13}O and ^{23}Si, the decay mode has not been seen so far. Most searches have concentrated on seeing particle emission from the IAS in the beta-daughter due to the large beta-strength to this state.

The case of ^{9}C is special in that all states populated in the beta-daughter ^{9}B break-up into two α-particles and a proton, see [12] and references therein. This could be presented as a 100% branching ratio for $\beta p\alpha$ or $\beta\alpha p$ decay to ^{4}He, but the decays of the $A = 9$ nuclei are special in several aspects [1,2] and are not typical for this decay mode.

Although $\beta p\alpha$ has not been observed so far for ^{13}O it must occur since β-decays to the IAS in ^{13}N have been observed [13] and close to half of the IAS decays are known from reaction experiments [14] to go via proton-emission to α unbound states in ^{12}C or α-emission to proton unbound states in ^{9}B. Actually, the final state in both cases will be a proton and three α-particles which makes the decay more challenging to observe. The total branching ratio for the decay mode can be estimated to be $0.9(3) \cdot 10^{-4}$.

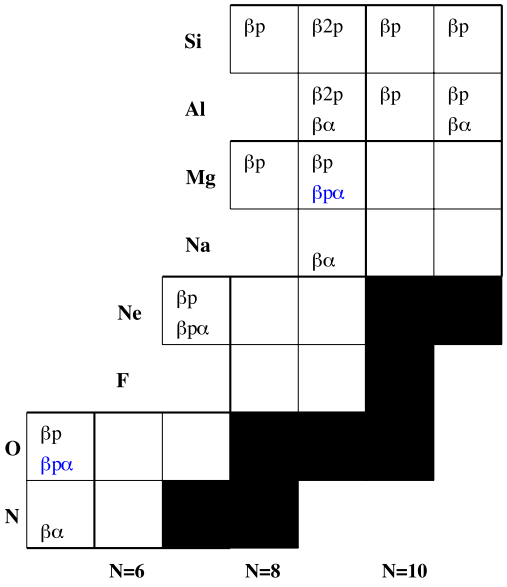

Fig. 4. (Color online.) The β^+-decaying isotopes of the elements from N to Si. Dark squares indicate stable isotopes. The experimentally observed beta-delayed particle decay modes are indicated, the $\beta p\alpha$ decay modes for ^{21}Mg (seen for the first time here) and ^{13}O (see Section 3.1) are marked in blue.

For ^{17}Ne both decay orderings, $\beta p\alpha$ and $\beta\alpha p$, have been observed [15] with a total branching ratio for the decay mode of $1.6(4) \cdot 10^{-4}$. All observed decays proceed through the IAS in ^{17}F and go to the final nucleus ^{12}C.

Adding now our observation of ^{21}Mg$(\beta p\alpha)^{16}$O it is striking that all cases go through an α-conjugate nucleus, namely ^{8}Be, ^{12}C, ^{16}O and ^{20}Ne respectively. Before drawing any firm structure conclusions we shall consider the broader systematics of beta-delayed particle emission in $Z > N$ nuclei.

3.2. Systematics of beta-delayed decays

Similar patterns also appear in other beta-delayed particle decays (see [1,9] for more data and for references to the original work). One closely related example is $\beta\alpha$ decays that occur for all bound $A = 4n$, $T_z = -1$ nuclei up to $A = 40$: ^{8}B, ^{12}N, ^{20}Na, ^{24}Al, ^{28}P, ^{32}Cl, ^{36}K and ^{40}Sc. The βp decays are well established [1] to occur strongly in $A = 4n + 1$, $T_z = -3/2$ nuclei. The $\beta 2p$ decays of ^{22}Al and ^{26}P and the $\beta 3p$ decay of ^{31}Ar [16] also all end up in an α-conjugate nucleus. The decays observed for the elements N to Si are shown in Fig. 4. Note that the $\beta\alpha$ and βp modes are not marked explicitly when the $\beta p\alpha$ or $\beta 2p$ modes also occur.

In the following we shall argue that the observed patterns are likely (except for the very lightest nuclei) to be related to odd–even effects rather than α-cluster structure. We start by considering the systematics of Q_{EC}-values for nuclei with $Z > N$ as illustrated in Fig. 5. Even though many effects contribute to the masses in this region, a liquid drop estimate reproduces the trend of Q_{EC} for the odd-A nuclei with $T_z = -1/2$ (dashed line) where only the Coulomb term enters, as well as for $T_z = -3/2$ (dotted line) where the asymmetry term also contributes. Note that Q_{EC} in the latter case varies little for A between 25 and 50.

The experimental data show that the Q_{EC}-values are roughly the same for each "quartet" of four nuclei that, as illustrated in

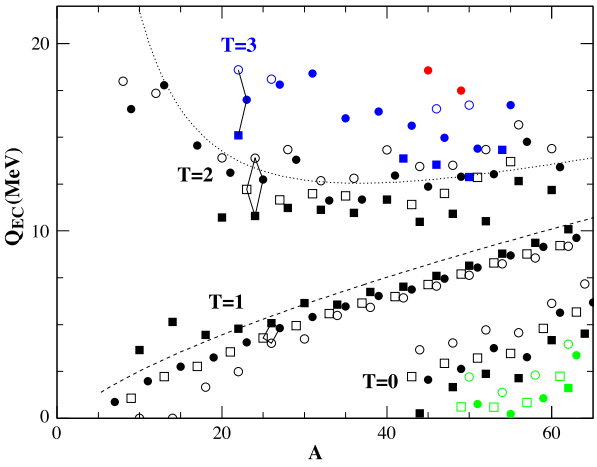

Fig. 5. (Color online.) Q_{EC} values for nuclei up to Ge. Filled symbols indicate nuclei with even Z, open symbols odd Z. Squares indicate nuclei with even N, circles odd N. The isospin values given are for the even–even nuclei. The green and red symbols correspond to $T = 1$ ($T_z = 1$) and $T = 4$. The dashed (dotted) line is a liquid drop estimate of Q_{EC} for nuclei with $T_z = -1/2$ ($-3/2$). The full lines indicate quartets of Al-Si nuclei.

	N	N+1
Z	e-e T	e-o T-1/2
Z-1	o-e T-1/2	o-o T-1

β3p	βp	βp βpα
β2p		βα

Fig. 6. Left part: The quartet of nuclei with similar Q-value. Right part: the favored beta-delayed decay modes. See the text for details.

the left panel of Fig. 6, have proton and neutron numbers (Z, N), (Z, N + 1), (Z − 1, N), (Z − 1, N + 1) where both Z and N are even. This is pronounced for quartets where the even–even nucleus has $T = 1$, and holds to a lesser degree also for $T = 2$ for mass numbers up to 40. The reason for this is that the two odd-A nuclei are at the same distance from the beta-stability line and therefore have about the same Q-value, as also shown by the liquid drop estimate. Without a pairing term in the liquid drop formula the Q-value for the even–even nucleus would be larger and the odd–odd smaller, but the odd–even effects counteracts this and as can be seen from Fig. 5 the magnitudes are even reversed for most nuclei. For the quartet with $T = 1$ (and $T_z = -1$) the odd–odd nucleus has $N = Z$ and is therefore extra bound, this happens to result in Q-values that are almost the same for all four nuclei. The quartets are indicated in Fig. 4 by thicker lines.

The observed decay patterns now follow from the energetics and are illustrated in the right panel of Fig. 6. The $\beta\alpha$ decays should occur in odd–odd nuclei, since they have slightly higher Q-values and the daughter alpha particle separation energies tend to be smallest here. The βp decays need low proton separation energies in the daughter nucleus and therefore are more prominent for even Z, starting (as one goes from stability towards the proton dripline) in an even–odd nucleus. The βpα decay should be favored in even–odd nuclei, and β2p and β3p decays should occur in odd–odd and even–odd nuclei, respectively, by extending these arguments.

Experimentally, the $\beta\alpha$, βp and βpα decays appear first in the quartets where the even–even nucleus has $T = 2$ and the odd–odd nucleus $T = 1$, but βp occurs also in ^{59}Zn, ^{65}Ge and heavier nuclei. The beta-delayed multi-proton decays appear in more exotic nuclei, but it is noteworthy that $\beta\alpha$ in these nuclei only has been observed in the odd–odd ^{22}Al.

Similar patterns can be expected for β^--delayed particle decays, although the grouping of Q-values is less pronounced here. The $\beta\alpha$ and βnα decay modes will in general occur further away from the beta-stability line.

4. Conclusion

Our study of the decay of ^{21}Mg has given the first evidence for the occurrence of the $\beta\alpha$ and βpα decay modes in this nucleus. The assignment of these decay modes to ^{21}Mg has been verified through statistical tests of the time distribution of the events. The occurrence of these decay modes in the β^+ decay of ^{21}Mg fits naturally into the systematics of previously observed β^+-delayed decays. We presented a brief overview of this systematics and argued that it can be explained by the variation in decay energy due to odd–even effects and that there is no need to invoke specific structure effects such as alpha-clustering in spite of α-conjugate nuclei occurring often as final state nuclei.

This interpretation can be tested when new instances of these exotic decays are discovered. The βpα decay mode may not occur in heavier $T_z = -3/2$ nuclei than ^{21}Mg (the Q-value becomes more than 10 MeV in ^{61}Ge, but the Coulomb barrier for α-particle emission is substantial then), but may be found also in the $T_z = -5/2$ nuclei ^{23}Si, ^{27}S, ^{31}Ar etc. If found in ^{20}Mg it may help to quantify the ^{15}O$(\alpha,\gamma)^{19}$Ne reaction rate [17]. A general overview of which energetically allowed decays have not yet been observed was given in [1].

Acknowledgements

We acknowledge support from the European Union Seventh Framework through ENSAR (contract no. 262010) and by the Spanish research agency under number FPA2012-32443. We thank Oliver Kirsebom for discussions.

References

[1] B. Blank, M.J.G. Borge, Prog. Part. Nucl. Phys. 60 (2008) 403.
[2] M. Pfützner, L.V. Grigorenko, M. Karny, K. Riisager, Rev. Mod. Phys. 84 (2012) 567.
[3] M.V. Lund, M.J.G. Borge, J.A. Briz, J. Cederkäll, H.O.U. Fynbo, J.H. Jensen, B. Jonson, K.L. Laursen, T. Nilsson, A. Perea, V. Pesudo, K. Riisager, O. Tengblad, Eur. Phys. J. A 51 (2015) 113.
[4] J.F. Ziegler, SRIM, http://srim.org/.
[5] R.G. Sextro, R.A. Gough, J. Cerny, Phys. Rev. C 8 (1973) 258.
[6] J.-C. Thomas, PhD thesis, University of Bordeaux, 2003.
[7] K.L. Laursen, O.S. Kirsebom, H.O.U. Fynbo, A. Jokinen, M. Madurga, K. Riisager, A. Saastamoinen, O. Tengblad, J. Äystö, Eur. Phys. J. A 49 (2013) 79.
[8] W. Gruhle, B. Kober, Nucl. Phys. A 286 (1977) 523.
[9] G. Audi, F.G. Kondev, M. Wang, B. Pfeiffer, X. Sun, J. Blachot, M. MacCormick, Chin. Phys. C 36 (2012) 1157.
[10] M.A. Stephens, in: R.B.D'Agostino, M.A. Stephens (Eds.), Goodness-of-Fit Techniques, Marcel Dekker, New York, 1986, p. 97.
[11] V. Choulakian, R.A. Lockhart, M.A. Stephens, Can. J. Stat. 22 (1994) 125.
[12] E. Gete, L. Buchmann, R.E. Azuma, D. Anthony, N. Bateman, J.C. Chow, J.M. D'Auria, M. Dombsky, U. Giesen, C. Iliadis, K.P. Jackson, J.D. King, D.F. Measday, A.C. Morton, Phys. Rev. C 61 (2000) 064310.
[13] H.H. Knudsen, H.O.U. Fynbo, M.J.G. Borge, R. Boutami, P. Dendooven, C.Aa. Diget, T. Eronen, S. Fox, L.M. Fraile, B. Fulton, J. Huikary, H.B. Jeppesen, A.S. Jokinen, B. Jonson, A. Kankainen, I. Moore, A. Nieminen, G. Nyman, H. Penttilä, K. Riisager, S. Rinta-Antila, O. Tengblad, Y. Wang, K. Wilhelmsen, J. Äystö, Phys. Rev. C 72 (2005) 044312.
[14] F. Ajzenberg-Selove, Nucl. Phys. A 523 (1991) 1.
[15] J.C. Chow, J.D. King, N.P.T. Bateman, R.N. Boyd, L. Buchmann, J.M. D'Auria, T. Davinson, M. Dombsky, E. Gete, U. Giesen, C. Iliadis, K.P. Jackson, A.C. Morton, J. Powell, A. Shotter, Phys. Rev. C 66 (2002) 064316.
[16] G.T. Koldste, B. Blank, M.J.G. Borge, J.A. Briz, M. Carmona-Gallardo, L.M. Fraile, H.O.U. Fynbo, J. Giovinazzo, J.G. Johansen, A. Jokinen, B. Jonson, T. Kurturkian-Nieto, T. Nilsson, A. Perea, V. Pesudo, E. Picado, K. Riisager, A. Saastamoinen, O. Tengblad, J.-C. Thomas, J. Van de Walle, Phys. Lett. B 737 (2014) 383.
[17] C. Wrede, Proceedings of XIII Nuclei in the Cosmos, PoS (NIC XIII) 039, 2014.